

NEUROSCIENCE

Targeting ischemia-induced KCC2 hypofunction rescues refractory neonatal seizures and mitigates epileptogenesis in a mouse model

Brennan J. Sullivan¹, Pavel A. Kipnis¹, Brandon M. Carter¹, Li-Rong Shao², Shilpa D. Kadam^{1,3*}

Copyright © 2021
The Authors, some
rights reserved;
exclusive licensee
American Association
for the Advancement
of Science. No claim
to original U.S.
Government Works

Neonatal seizures pose a clinical challenge in their early detection, acute management, and long-term comorbidities. They are often caused by hypoxic-ischemic encephalopathy and are frequently refractory to the first-line anti-seizure medication phenobarbital. One proposed mechanism for phenobarbital inefficacy during neonatal seizures is the reduced abundance and function of the neuron-specific K⁺/Cl⁻ cotransporter 2 (KCC2), which maintains chloride homeostasis and promotes GABAergic inhibition upon its phosphorylation during postnatal development. Here, we investigated whether this mechanism is causal and whether it can be rescued by KCC2 functional enhancement. In a CD-1 mouse model of refractory ischemic neonatal seizures, treatment with the KCC2 functional enhancer CLP290 rescued phenobarbital efficacy, increased KCC2 abundance, and prevented the development of epileptogenesis, as quantified by video electroencephalogram monitoring. These effects were prevented by knock-in expression of nonphosphorylatable mutants of KCC2 (S940A or T906A and T1007A), indicating that KCC2 phosphorylation regulates both neonatal seizure susceptibility and CLP290-mediated KCC2 functional enhancement. Our findings therefore validate KCC2 as a clinically relevant target for refractory neonatal seizures and provide insights for future drug development.

INTRODUCTION

Neonatal seizures occur in an estimated 1 to 3.5 per 1000 live births in the term infant. Hypoxic-ischemic encephalopathy is a major cause of acute neonatal seizures (1). The management of these seizures is a major clinical challenge, because they are often refractory to an initial loading dose of the first-line antiseizure medication (ASM) phenobarbital (PB) and adjunct ASMs (2, 3). Compared to seizures at older ages, neonatal seizures differ in their etiology, semiology, electrographic signature, and response to ASMs (1, 4). There is an urgent need to identify the developmental mechanisms underlying seizure susceptibility and ineffective ASM response in the neonatal brain.

The neonatal brain has low expression of its chief chloride extruder the neuron-specific K⁺-Cl⁻ cotransporter 2 (KCC2) and a high neuronal intracellular chloride concentration ([Cl⁻]_i) (5, 6). γ-Aminobutyric acid (GABA) is the primary inhibitory neurotransmitter in the mature brain; however, in the neonatal brain, the activation of GABA type A receptors (GABARs) results in depolarizing actions on immature neurons (7). KCC2 expression and function increase during development, resulting in a lower [Cl⁻]_i that coincides with a developmental shift from depolarizing to hyperpolarizing GABAergic signaling. The importance of KCC2 function in seizure susceptibility is supported by emerging evidence from human genetics, as pathogenic variants in SLC12A5 are associated with the development of idiopathic generalized epilepsy and early infantile epileptic encephalopathy [Online Mendelian Inheritance in Man (OMIM) #616685 and #616645, respectively] (8).

Despite the introduction of many new ASMs into clinical practice over the past 20 years, the incidence of refractory seizures has remained unchanged (9). KCC2 hypofunction is increasingly associated with pharmacoresistant epilepsies and is a proposed cause of disinhibition (10, 11). GABA_AR-mediated fast synaptic inhibition and the antiseizure efficacy of PB (a positive allosteric modulator of GABA_ARs) are both dependent upon active neuronal Cl⁻ extrusion (12, 13). In a preclinical CD-1 mouse model of ischemic neonatal seizures, KCC2 is transiently down-regulated and associated with PB-resistant seizures (14). In this model, post-ischemic inhibition of tropomyosin receptor kinase (TrkB) rescued PB-resistant neonatal seizures and KCC2 expression (15, 16). This acute rescue of KCC2 hypofunction by TrkB inhibition improved long-term outcomes after ischemic neonatal seizures (17–19). These results suggest that KCC2 is a novel therapeutic target for refractory neonatal seizures.

A published high-throughput screen for compounds that reduce [Cl⁻]_i in a cell line with low KCC2 expression identified the compound CLP257 as a KCC2 functional enhancer (20). Here, we used CLP257 and the carbamate prodrug CLP290 (20) in a well-characterized CD-1 mouse model and S940A^{+/+} and T1007A^{+/+} point-mutation mice to test whether functional enhancement of KCC2 can rescue the emergence of PB-resistant ischemic neonatal seizures, whether there are differences in their efficacy corresponding to developmental changes in KCC2 expression (14), whether they can prevent the development of epilepsy associated with neonatal seizures (21, 22), and whether these effects are dependent on development-associated KCC2 phosphorylation (23–26).

RESULTS

CLP290 rescues PB-resistant seizures at P7

The true burden of acute ischemic seizures in mouse pups cannot be identified by behavioral scoring parameters alone and requires

¹Neuroscience Laboratory, Hugo Moser Research Institute at Kennedy Krieger, Baltimore, MD, USA. ²Division of Pediatric Neurology, Department of Neurology, Johns Hopkins University School of Medicine, Baltimore, MD, USA. ³Department of Neurology, Johns Hopkins University School of Medicine, Baltimore, MD 21205, USA.

*Corresponding author. Email: kadam@kennedykrieger.org

continuous video electroencephalography (vEEG) recordings, because their presentation can range from entirely electrographic to generalized convulsive (5). In this CD-1 mouse model of unilateral carotid ligation without transection, pups presented with PB-resistant ischemic neonatal seizures at postnatal day 7 (P7) (Fig. 1, A to D), an established characteristic of the model (14–16, 27). This model represents transient ischemia followed by reperfusion that results in cerebral edema at 24 hours with no discernable infarcts when evaluated at P18 (14). All pups underwent 1 hour of baseline vEEG recording after unilateral carotid ligation. After that hour, all pups received a loading dose of PB with a subsequent hour of vEEG recording (Fig. 1, A to D). Pups that only received a PB-loading dose were resistant to PB, given that their second-hour seizure burden remained high and was similar to first-hour levels (Fig. 1D and fig. S1, A and B).

To investigate whether the KCC2 functional enhancer CLP290 could rescue PB-resistant seizures, CLP290 was administered intraperitoneally to P7 pups in three groups: “pre” (treated with the specified dose—5, 10, or 20 mg/kg—4 hours before ligation), “post” (treated immediately after ligation), and “primed” (both 4 hours before ligation and immediately after ligation) (Fig. 1B). Administration of CLP290 (10 mg/kg; i.p.) to P7 pups 4 hours before ligation (primed treatment; referred to as 10' in the figures) significantly reduced total burden, duration, and frequency of second-hour seizure events (Fig. 1D and fig. S1, A and B) and significantly increased seizure suppression after PB administration, thereby rescuing P7 PB resistance (Fig. 1D). In contrast to the 10' treatment, bolus administration of 20'' [CLP290 (20 mg/kg) for 4 hours before ligation] reduced first-hour baseline seizure burden (fig. S1C).

Bioavailability of the prodrug CLP290 in the neonatal mouse brain

A major limiting factor for epilepsy drug development is the *in vivo* brain availability of candidate compounds identified *in vitro* (28, 29). CLP290 is a carbamate prodrug of CLP257 and has an improved half-life ($t_{1/2}$) from <15 min (CLP257) to 5 hours (CLP290) in blood samples from adult rats (20). At P7, CLP257 was unable to reduce second-hour seizure burden (Fig. 1, E and F, and fig. S1, D and E) when administered systemically at the 10' dose likely due to its poor $t_{1/2}$. To our knowledge, the brain bioavailability of systemically administered CLP290 in neonatal mice is not yet reported. To determine whether CLP290 antiseizure efficacy was associated with brain bioavailability at 4 hours, we performed high-performance liquid chromatography (HPLC) to analyze brain and plasma levels of CLP290 after intraperitoneal delivery. In addition, the metabolism of CLP290 into its active form CLP257, in the plasma and brain, at 4 hours was also quantified in the same samples (Fig. 1, G to I, and fig. S2). At P7 and P10, CLP290 administration of 10 or 20 mg/kg demonstrated adequate brain bioavailability at 4 hours (Fig. 1H). The concomitant CLP257 brain-plasma ratios were lower compared to the prodrug CLP290 (Fig. 1I).

To further investigate the effect of CLP290, naïve CD-1 pups underwent CLP290 10' treatment, and the cortices were harvested for Western blot analysis 4 hours later (fig. S3, A to D). CLP290 did not significantly increase total KCC2 or Ser⁹⁴⁰ phosphorylation levels at either P7 or P10 in naïve cortex. These results demonstrate that CLP290 10' was readily bioavailable in the P7 neonatal brain at 4 hours after systemic delivery, and CLP290 10' did not significantly increase total KCC2 and Ser⁹⁴⁰ phosphorylation in naïve brains

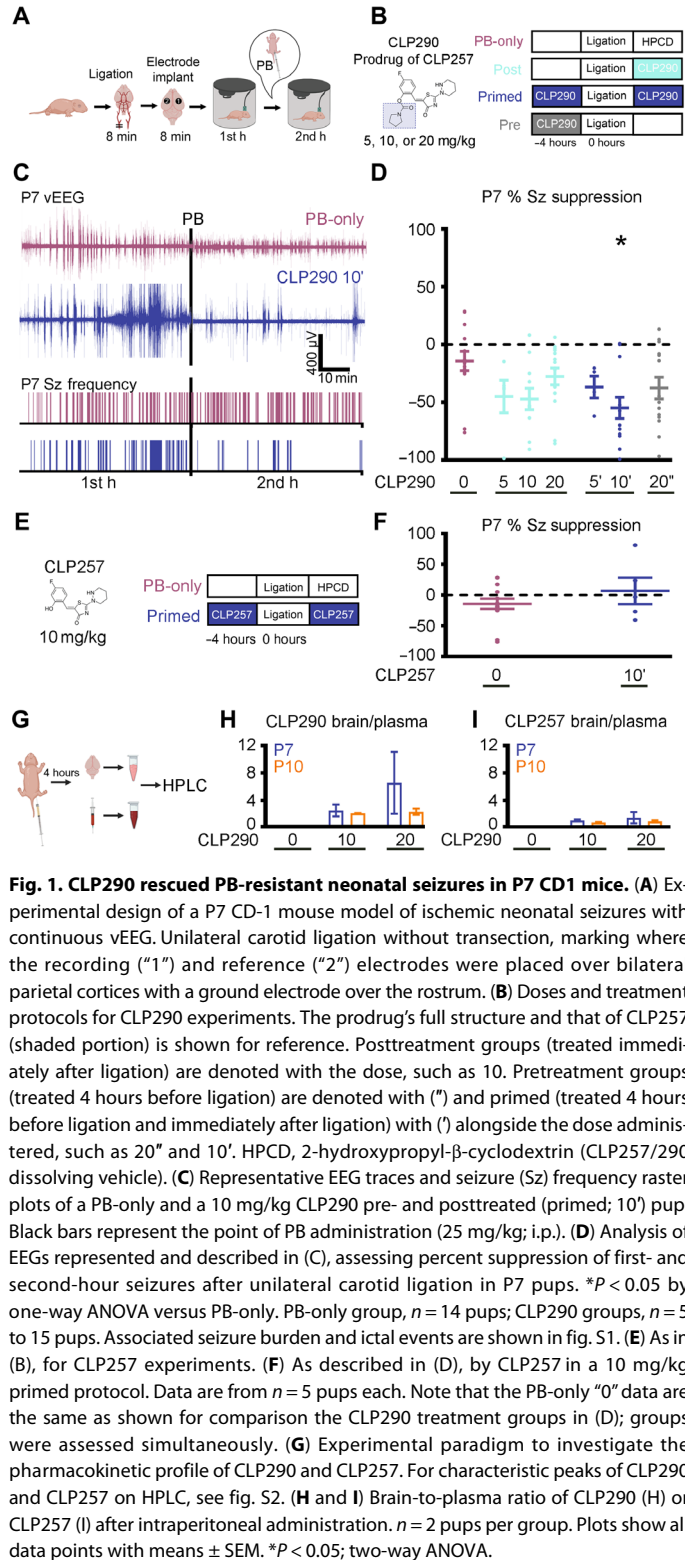


Fig. 1. CLP290 rescued PB-resistant neonatal seizures in P7 CD1 mice. (A) Experimental design of a P7 CD-1 mouse model of ischemic neonatal seizures with continuous vEEG. Unilateral carotid ligation without transection, marking where the recording (“1”) and reference (“2”) electrodes were placed over bilateral parietal cortices with a ground electrode over the rostrum. (B) Doses and treatment protocols for CLP290 experiments. The prodrug’s full structure and that of CLP257 (shaded portion) is shown for reference. Posttreatment groups (treated immediately after ligation) are denoted with the dose, such as 10. Pretreatment groups (treated 4 hours before ligation) are denoted with (') and primed (treated 4 hours before ligation and immediately after ligation) with (") alongside the dose administered, such as 20'' and 10''. HPCD, 2-hydroxypropyl-β-cyclodextrin (CLP257/290 dissolving vehicle). (C) Representative EEG traces and seizure (Sz) frequency raster plots of a PB-only and a 10 mg/kg CLP290 pre- and posttreated (primed; 10') pup. Black bars represent the point of PB administration (25 mg/kg; i.p.). (D) Analysis of EEGs represented and described in (C), assessing percent suppression of first- and second-hour seizures after unilateral carotid ligation in P7 pups. * P < 0.05 by one-way ANOVA versus PB-only. PB-only group, n = 14 pups; CLP290 groups, n = 5 to 15 pups. Associated seizure burden and ictal events are shown in fig. S1. (E) As in (B), for CLP257 experiments. (F) As described in (D), by CLP257 in a 10 mg/kg primed protocol. Data are from n = 5 pups each. Note that the PB-only “0” data are the same as shown for comparison the CLP290 treatment groups in (D); groups were assessed simultaneously. (G) Experimental paradigm to investigate the pharmacokinetic profile of CLP290 and CLP257. For characteristic peaks of CLP290 and CLP257 on HPLC, see fig. S2. (H and I) Brain-to-plasma ratio of CLP290 (H) or CLP257 (I) after intraperitoneal administration. n = 2 pups per group. Plots show all data points with means \pm SEM. * P < 0.05; two-way ANOVA.

with the same protocol. In summary, these results suggest that the therapeutic effect of CLP290-mediated functional KCC2 enhancement is beneficial when it is bioavailable at the onset of KCC2 hypofunction after the ischemic insult and does not depend on increasing the total expression KCC2 by pretreatment.

CLP290 efficacy on PB-responsive seizures at P10

As previously reported (14–16, 27), ischemic neonatal seizures after unilateral carotid ligation in P10 CD-1 pups were PB responsive (Fig. 2, A to C). The age-dependent emergence of PB-resistant and PB-responsive seizures at P7 versus P10 is a characteristic of the CD-1 neonatal mouse model that is associated with an increase in KCC2 expression between P7 and P10 (14). Administration of CLP290 at P10 did not further improve the efficacy of PB at any of the doses tested (Fig. 2C and fig. S1, F and G). When ischemic neonatal seizures were PB responsive at P10, the previously reported TrkB antagonist ANA12 (16, 27) also did not improve the efficacy of PB. This suggests that the therapeutic benefit of KCC2 functional enhancement is dependent upon the degree of KCC2 hypofunction, which is evident in the emergence of refractoriness at P7 but not at P10.

Acute CLP290 intervention at P7 mitigates epileptogenesis at P12

Hypoxic-ischemic encephalopathy seizures are transient within the first week of life (30, 31), and the long-term consequences of neonatal seizures are difficult to isolate from the consequences of prolonged and/or ineffectual antiseizure therapy in the clinic (22). In this CD-1 mouse model of refractory neonatal ischemic seizures, we have previously documented the emergence of epilepsy in adulthood (17). To assess whether the acute rescue of PB-resistant neonatal seizures at P7 by administration of CLP290 had long-term benefits, the same pups underwent a pentylenetetrazole (PTZ) challenge at P12 (Fig. 3, A and B). Previously, an 80 mg/kg dose of the GABA_AR antagonist PTZ was shown to induce high seizure burdens that were PB responsive and up-regulated KCC2 at P7 in CD-1 pups (32). In this study, pups were administered three doses of PTZ (20, 20, and 40 mg/kg) 1 hour apart (Fig. 3, A and B). Using this protocol, we characterized seizure susceptibility in P7 naïve, P7 PB-only, and P7 CLP290 10'-treated pups at P12. The initial dose of PTZ induced seizures in the first hour for all groups (Fig. 3, A to D). Naïve pups demonstrated a general reduction in seizures during the second and third PTZ doses, potentially uncovering a homeostatic compensation to help develop resistance to the chemoconvulsant-induced seizures. PB-only pups demonstrated an increase in seizure burden after the repeated doses of PTZ, with mice going into status epilepticus (Fig. 3, D to F). Thus, the increase in PB-only seizure

burdens at P12 was driven by a significant increase in seizure duration (Fig. 3E). CLP290 10'-treated pups had similar P12 seizure burdens as naïve pups and significantly lower than PB-only pups (Fig. 3, A to D). This PTZ challenge protocol identified epileptogenesis in the form of heightened susceptibility to seizures at P12 for neonatal pups that underwent standard but ineffectual PB treatment for their refractory seizures at P7. The efficacious CLP290 10' intervention at P7 resulted in the regression of epileptogenesis at P12.

Hyperexcitability after suppression of GABA_AR-mediated inhibition has been demonstrated in ex vivo brain slices from experimental models of epilepsy in adulthood (33–36). To determine whether the in vivo PTZ (GABA_AR antagonist) challenge represented progressive electrophysiological changes underlying hyperexcitability after P7 ischemic seizures, ex vivo coronal neocortical slices from the ipsilateral cortex of CD-1 mice 5 to 8 days after ischemic seizures (P12 to P15) were investigated in both normal artificial cerebral spinal fluid (ACSF) and after blockade of GABA_ARs with GABAazine. Evoked field potentials (EFPs) were recorded in frontal and posterior sections (Fig. 3, G to I) representing the perfusion territories of the anterior and middle cerebral arteries with and without collateral circulation in this model (33). Brain slices from the posterior neocortex in PB-only pups demonstrated a significantly reduced latency to threshold (Fig. 3, J and K), which was not detected in their anterior brain slice. In normal ACSF, EFPs in both frontal and posterior sections were similar between naïve and PB-only pups, and the responses remained graded from EFP threshold to six times EFP threshold, 1T to 6T (Fig. 3, L and M). In contrast, blockade of GABA_ARs with GABAazine resulted in larger amplitude EFPs that lacked a graded response in the frontal sections from PB-only mice (Fig. 3, L and M). In contrast, ex vivo sections from naïve mice demonstrated no significant differences between EFPs in normal ACSF and GABA_AR blockade (Fig. 3L). The in vivo PTZ challenge and ex vivo EFP results both suggest that GABAergic electrophysiological changes mask underlying hyperexcitability at P12 to P15 after P7 ischemic seizures and become evident when GABA_ARs were antagonized either by GABAazine in vitro or PTZ in vivo.

Spontaneous epileptiform discharges in S940A^{+/+} pups

The chloride extrusion capacity of KCC2 is greatly influenced by the phosphorylation status of residues Ser⁹⁴⁰ and Thr¹⁰⁰⁷ (23–25). KCC2 phosphomutant mice enabled the investigation of the role of these residues in the emergence of refractory seizures at neonatal ages. It is already known that KCC2-deficient mice die postnatally with generalized seizures and respiratory failure (37, 38). S940A^{+/+} mice are susceptible to death after kainite-induced status epilepticus in adulthood (25). In patients with idiopathic generalized epilepsy and early childhood onset of febrile seizures, heterozygous missense variants in SLC12A5 have been identified (39, 40) and associated with a reduction in Ser⁹⁴⁰ phosphorylation (39). However, it is not currently reported whether the prevention of Ser⁹⁴⁰ phosphorylation

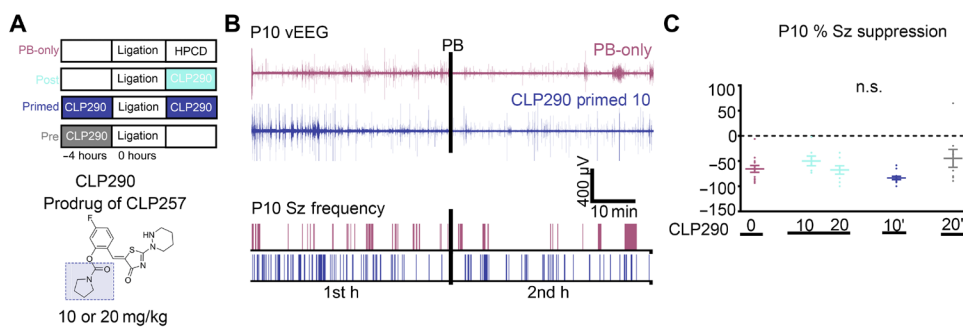
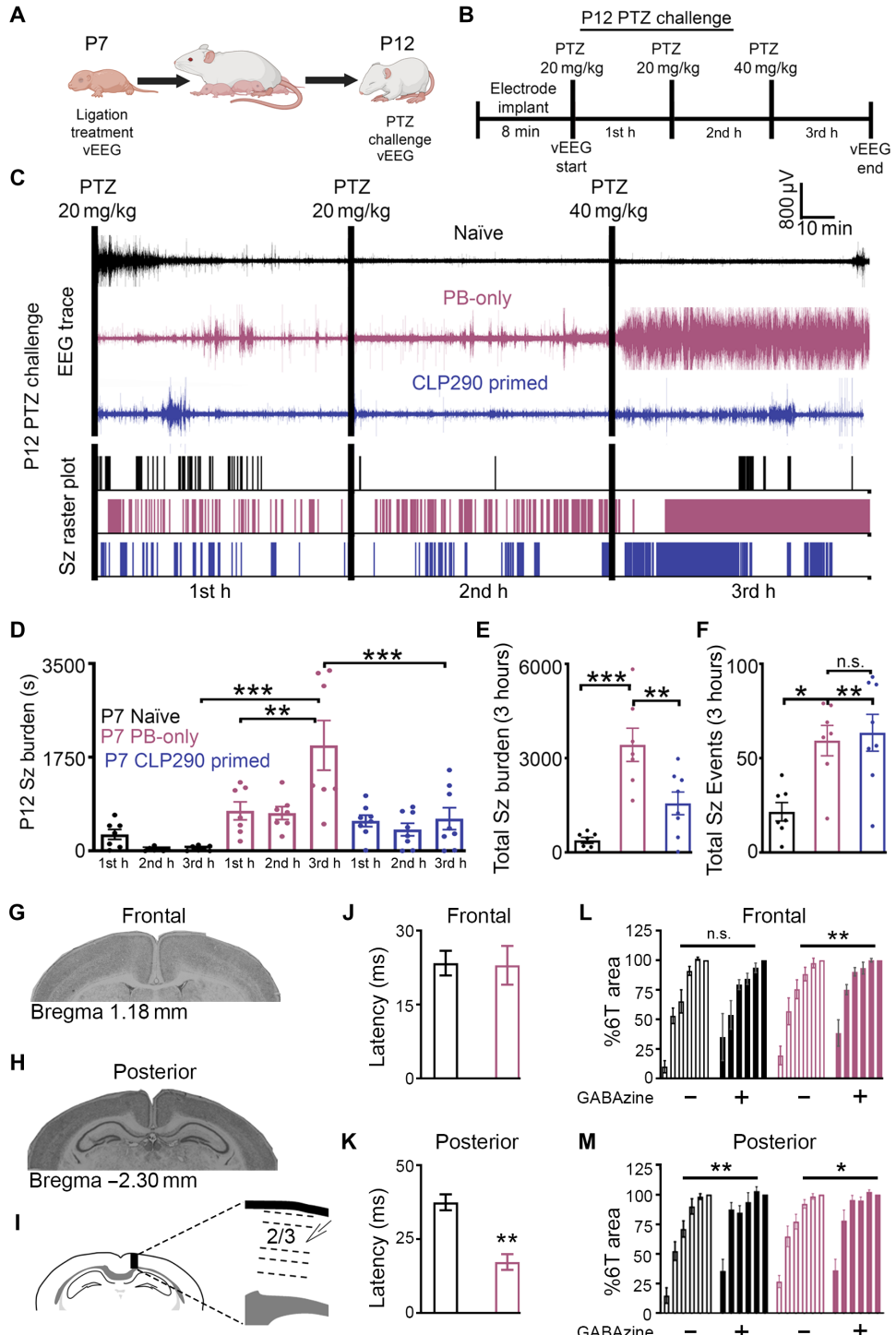


Fig. 2. Ischemic neonatal seizures in P10 CD1 pups were PB-responsive. (A) Doses and treatment protocols to evaluate CLP290 in P10 CD-1 pups. (B) Representative EEG traces and seizure frequency raster plots of a P10 PB-only and CLP290 10' pup. Black bars represent a loading dose of PB (25 mg/kg, i.p.). (C) First- and second-hour percent seizure suppression at P10 after unilateral carotid ligation. Percent seizure suppression was analyzed by one-way ANOVA versus PB-only. PB-only, $n = 13$; CLP290 10', $n = 7$; CLP290 20', $n = 8$; CLP290 10'', $n = 12$; CLP290 20'', $n = 8$ pups. For first- and second-hour seizure burden and ictal events, see fig. S1. n.s., not significant.

Fig. 3. CLP290-mediated regression of epileptogenesis detected using a PTZ challenge. (A) Schematic to investigate the developmental benefits of CLP290 10' treatment for P7 ischemic seizures. (B) P12 pentylenetetrazol (PTZ) challenge to evaluate epileptogenesis. (C) Representative EEG traces and seizure frequency raster plots for P12 pups that were untreated (naïve) or underwent PB-only or CLP290 10' treatment at P7. Black bars indicate intraperitoneal PTZ injections. (D) First-, second-, and third-hour seizure burdens at P12 in CD-1 mice after PTZ injections. (E) Total electrographic seizure burdens over the 3 hours of vEEG recording. (F) Total seizure events over 3 hours of vEEG recording. Data plots show all data points with means \pm SEM. * $P < 0.05$; ** $P < 0.01$; *** $P < 0.001$ by two-way ANOVA. Naïve, $n = 7$; PB-only, $n = 7$; CLP290 10', $n = 8$ mice. (G to I) Representative coronal sections from frontal (G) and posterior (H) recording areas; line diagram (I) shows the placement of the recording electrode in an intact cortical column from a posterior section. (J and K) Mean 1T latencies from frontal (J) and posterior (K) sections from P12 to P15 pups that were untreated (naïve) or PB-treated at P7. (L and M) Percent 6T area from frontal (L) and posterior (M) sections with and without GABAzine ($1 \mu\text{M}$). * $P < 0.05$, ** $P < 0.01$, and *** $P < 0.001$ by t test and two-way ANOVA. Naïve, $n = 7$; PB-only, $n = 14$ mice.



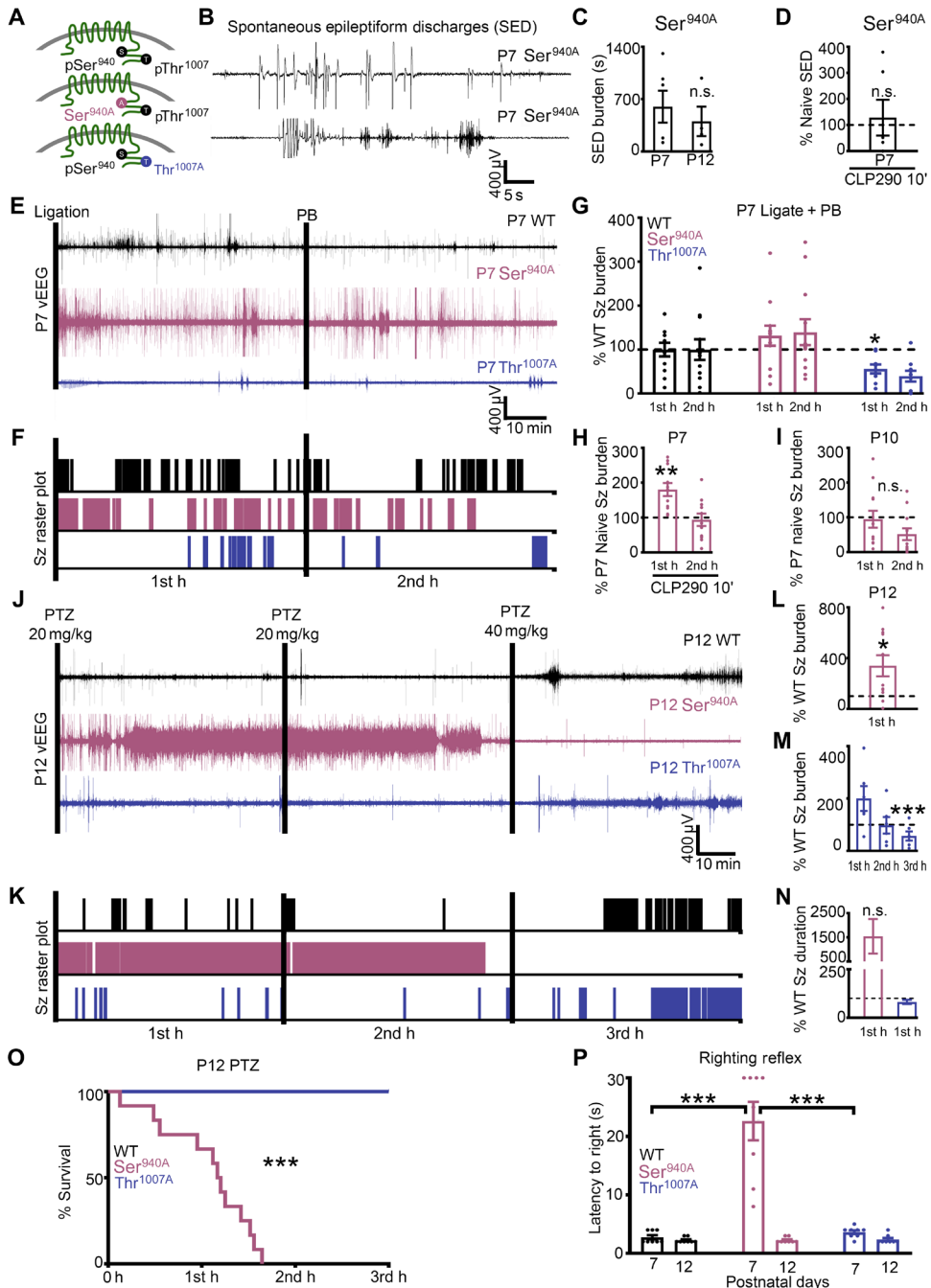
alone can induce spontaneous epileptiform activity during the neonatal period. Therefore, S940A^{+/+} pups underwent vEEG at P7 and P12 (Fig. 4, A to D). S940A^{+/+} mice had spontaneous epileptiform discharges at both P7 and P12, which failed to respond to CLP290 intervention (Fig. 4, A to D). These results suggest that the inability to phosphorylate the Ser⁹⁴⁰ residue engenders spontaneous epileptic activity during development.

T1007A^{+/+} pups are resistant to ischemic seizures

Thr¹⁰⁰⁷ phosphorylation decreases during development and is associated with an increase in neuronal Cl⁻ extrusion capacity (23, 26, 41). T1007A^{+/+} knock-in mutant mice have a reduced susceptibility to kainate-induced status epilepticus in adulthood (24). To investigate the role of KCC2 phosphorylation in ischemic neonatal seizures, wild-type (WT), S940A^{+/+}, and T1007A^{+/+} P7 pups underwent unilateral carotid ligation with 2 hours of vEEG recordings (Fig. 4, E to G). After P7 unilateral carotid ligation, T1007A^{+/+} pups were significantly resistant to ischemic seizures than WT (Fig. 4, E to G). This result suggests that reducing Thr¹⁰⁰⁷

phosphorylation on KCC2 is a promising therapeutic target. S940A^{+/+} pups had higher seizure burdens than WT after ischemia (Fig. 4G). CLP290 treatment for 10 min did not improve the efficacy of PB in S940A^{+/+} mice but significantly increased first-hour seizure burden when compared to untreated S940A^{+/+} mice (Fig. 4H). During development, mice undergo a reduction in ischemic seizure susceptibility from P7 to P10 that is associated with a robust up-regulation of KCC2 and Ser⁹⁴⁰ phosphorylation (14, 27). S940A^{+/+} mice did

Fig. 4. Inability to phosphorylate Ser⁹⁴⁰ or Thr¹⁰⁰⁷ in knock-in pups regulated neonatal seizure susceptibility. (A) Graphical representation of homozygous S940A knock-in mutant mice (26) and homozygous T1007A knock-in mutant mice (25). (B and C) S940A^{+/+} mice had spontaneous epileptiform discharges (SEDS) at P7 and P12. (D) Spontaneous epileptiform discharge duration of P7 S940A^{+/+} pups administered CLP290 10' treatment. Naïve P7 S940A^{+/+}, n = 6; naïve P12 S940A^{+/+}, n = 4; and CLP290 10' P7 S940A^{+/+}, n = 6 pups. (E to G) P7 T1007A^{+/+} pups are resistant to ischemic neonatal seizures. (E) EEG traces and (F) seizure frequency raster plots for P7 WT, S940A^{+/+}, and T1007A^{+/+} pups that underwent unilateral carotid ligation. (G) First- versus second-hour seizure burdens after unilateral carotid ligation, plotted as percent WT. WT, n = 12; S940A^{+/+}, n = 12; and T1007A^{+/+}, n = 9 pups. (H) P7 S940A^{+/+} ischemic seizures in response to CLP290 (10'). Seizure burden of CLP290 10' treated P7 S940A^{+/+} pups after unilateral carotid ligation plotted as P7 percent naïve S940A^{+/+}. CLP290 10'-treated P7 S940A^{+/+}, n = 11 pups. (I) Seizure burden of P10 S940A^{+/+} pups (n = 8) after unilateral carotid ligation, plotted as P7 percent naïve S940A^{+/+}. n.s., P = 0.57. (J to O) Naïve P12 S940A^{+/+} mice are susceptible to status epilepticus and mortality. (J) Representative EEG trace and (K) seizure frequency raster plot of naïve P12 WT, S940A^{+/+}, and T1007A^{+/+} pups. Black bars indicate intraperitoneal PTZ injections. (L) Total seizure burden of P12 S940A^{+/+} pups after PTZ administration plotted as percent WT. (M) First-, second-, and third-hour seizure burdens at P12 in T1007A^{+/+} pups plotted as percent WT. (N) first-hour average seizure durations for S940A^{+/+} and T1007A^{+/+} P12 pups, plotted as percent WT. (O) Survival plot for P12 WT, T1007A^{+/+}, and S940A^{+/+} pups during the PTZ challenge. P12 WT, n = 11; S940A^{+/+}, n = 11; and T1007A^{+/+}, n = 6 pups. (P) Duration of time to righting reflex at P7 and P12 in naïve WT, T1007A^{+/+}, and S940A^{+/+} pups (n = 8 pups each group). *P < 0.05; **P < 0.01; ***P < 0.001 by unpaired t test versus WT for all seizure data. Survival analysis, ***P < 0.001 by Mantel-Cox test. Righting reflex by one-way ANOVA.



not undergo a developmental decrease in ischemic seizure susceptibility at P10 when compared to P7 S940A^{+/+} mice (Fig. 4I). These results suggest that both the CLP290-mediated KCC2 functional enhancement and the age-dependent reduction in ischemic seizure susceptibility are dependent upon Ser⁹⁴⁰ phosphorylation.

S940A^{+/+} pups are susceptible to status epilepticus and death

WT, S940A^{+/+}, and T1007A^{+/+} pups at P12 underwent the 3-hour PTZ challenge to determine whether KCC2 phosphorylation status influenced seizure susceptibility independent of ischemia. As described above (Fig. 3), pups were administered three doses of PTZ

(20, 20, and 40 mg/kg) 1 hour apart. S940A^{+/+} mice immediately progressed into status epilepticus and died before the second hour (Fig. 4J to O). This indicated that the prevention of Ser⁹⁴⁰ phosphorylation increased the risk of sudden unexpected death in epilepsy-like phenomenon (42). In contrast, T1007A^{+/+} mice were resistant to the PTZ-induced seizures when compared to WT (Fig. 4M). In addition, the assessment of righting reflex as a neurodevelopmental milestone identified that only S940A^{+/+} mice had a significantly impaired righting reflex at P7 but not at P12 (Fig. 4P). These data suggest that KCC2 phosphorylation at residues Ser⁹⁴⁰ and Thr¹⁰⁰⁷ influence seizure susceptibility during development.

In vivo KCC2 inhibition is epileptogenic in the neonatal brain

Microinfusion of the selective KCC2 inhibitor VU0463271 (VU) has been shown to induce epileptiform discharges in the dorsal hippocampus of the adult mouse *in vivo* (43). During spontaneous recurrent ictal-like epileptiform discharges in organotypic hippocampal slices *in vitro*, VU reduced Cl^- extrusion rates and induced status epilepticus (44). These studies highlight the critical role of KCC2 in curbing epileptiform activity in the mature hippocampus. Here, naïve P7 CD-1 pups were administered VU (0.25 mg/kg; i.p.) at the initiation of vEEG recording with a subsequent dose of VU (0.5 mg/kg; i.p.) at 1 hour (Fig. 5, A and B). VU was sufficient to induce epileptiform activity (Fig. 5, A to E) at P7. Prolonged and repeated seizures are known to play a role in the reduction of neuronal surface KCC2 expression and function (15, 25, 45, 46). At P7, if post-ischemic KCC2 hypofunction plays a critical role in

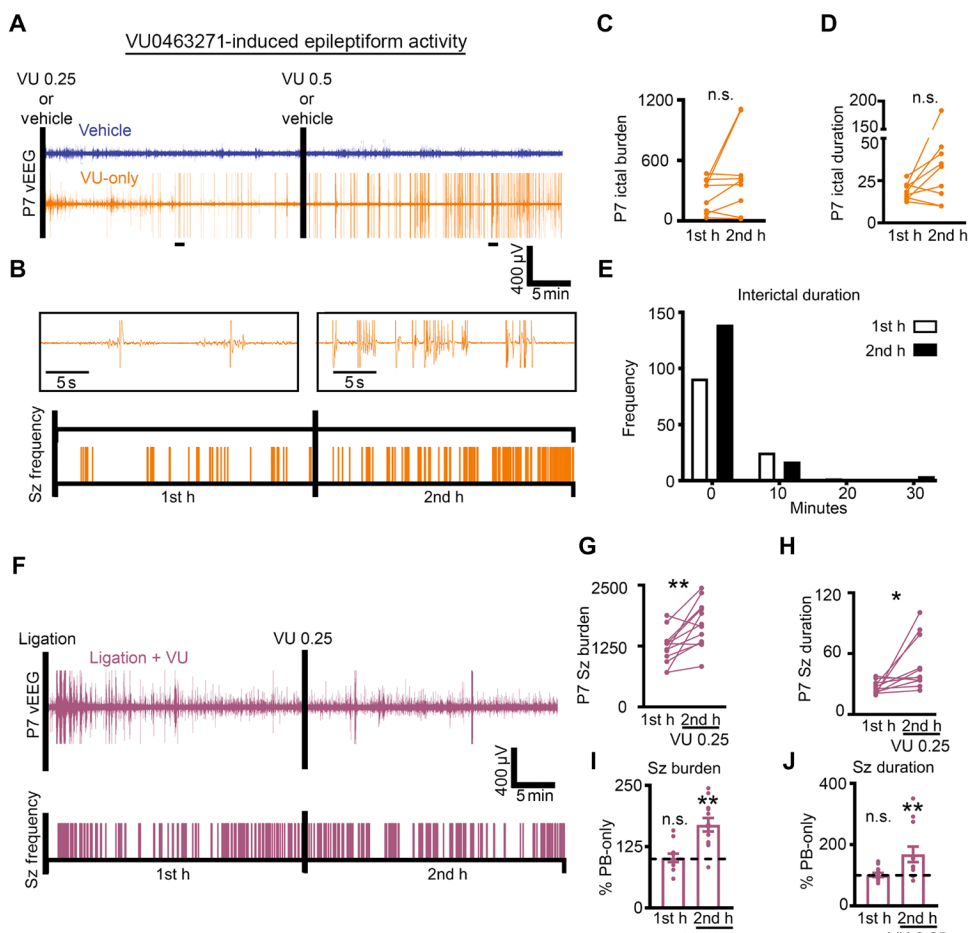


Fig. 5. Selective KCC2 antagonist VU induced spontaneous epileptiform discharges in P7 pups. (A to E) Representative EEG traces (A) and ictal event frequency raster plots (B) from P7 CD-1 pups that were administered either vehicle or VU0463271 (VU); black bars note intraperitoneal injections. Expanded time scales show VU-induced epileptiform activity in the first- and second-hour. First- versus second-hour ictal burden (C) and duration (D) after VU administration. Total frequency distribution for all interictal durations in P7 CD-1 pups administered VU (E). Vehicle, $n = 4$ pups; VU, $n = 8$ pups. (F to J) Representative EEG trace and seizure frequency raster plot (F) of P7 CD-1 pups that underwent unilateral carotid ligation with administration of VU of 0.25 mg/kg at 1 hour (denoted by black bar). First- and second-hour seizure burden (G) and duration (H). (I and J) First- and second-hour seizure burden and duration plotted as percent PB-only. Data plots show all data points with means \pm SEM. * $P < 0.05$ and ** $P < 0.01$ by two-tailed paired t test. Ligation + VU, $n = 12$ pups.

PB refractoriness, then KCC2 inhibition after repeated ischemic seizures would be expected to further aggravate the seizure burden. To test the effect of KCC2 inhibition after repeated ischemia-induced neonatal seizures at P7, VU (0.25 mg/kg; i.p.) was administered 1 hour after unilateral carotid ligation (Fig. 5F). P7 pups that received VU after 1 hour of ischemic seizures developed a significant aggravation of EEG seizure burden in the second hour (Fig. 5, F to J). Together, the data show that KCC2 inhibition induced epileptiform activity in the naïve neonatal brain and exacerbated ischemic neonatal seizures at P7.

CLP290 rescued ipsilateral post-ischemic KCC2 and Ser⁹⁴⁰ down-regulation

Excitotoxic injury results in deficits in KCC2 expression and activity (11, 13, 20, 45, 47–51). PB-resistant ischemic neonatal seizures have

been shown to significantly reduce expression of KCC2 and phosphorylation of Ser⁹⁴⁰ 24 hours after ischemia (16). P7 unilateral carotid ligation did not result in an infarct stroke injury, therefore KCC2 degradation at 24 hours is not caused by infarct related cell death (14). In this model, KCC2 expression undergoes a recovery over 3 to 4 days, a characteristic that is associated with the transient nature of neonatal seizures due to hypoxic-ischemic encephalopathy (30, 31). Twenty-four hours after P7 unilateral carotid ligation, KCC2 abundance and Ser⁹⁴⁰ phosphorylation was significantly lower in the right hemisphere (ipsilateral to ischemia) than in the left hemisphere (contralateral to ischemia) in the PB-only group (Fig. 6, A to E, and data file S1). Intervention with CLP290 at P7 significantly rescued both KCC2 and Ser⁹⁴⁰ down-regulation in the 10' group 24 hours after ligation (Fig. 6, B and C). After PB-responsive seizures at P10, KCC2 expression was not significantly decreased at 24 hours (Fig. 6, F to J, and data file S1). However, Ser⁹⁴⁰ phosphorylation in the PB-only group was significantly decreased (Fig. 6H) and was rescued by CLP290 treatment (Fig. 6H). Therefore, when ischemic neonatal seizures were PB-resistant, CLP290 rescued KCC2 expression and Ser⁹⁴⁰ phosphorylation, suggesting that the degree of KCC2 hypofunction drives the therapeutic benefit of KCC2 functional enhancement.

Ischemic neonatal seizures do not modulate KCC2-Thr¹⁰⁰⁷ phosphorylation

The phosphorylation of KCC2 residue Thr¹⁰⁰⁷ decreases KCC2 function (52, 53). It has been proposed that

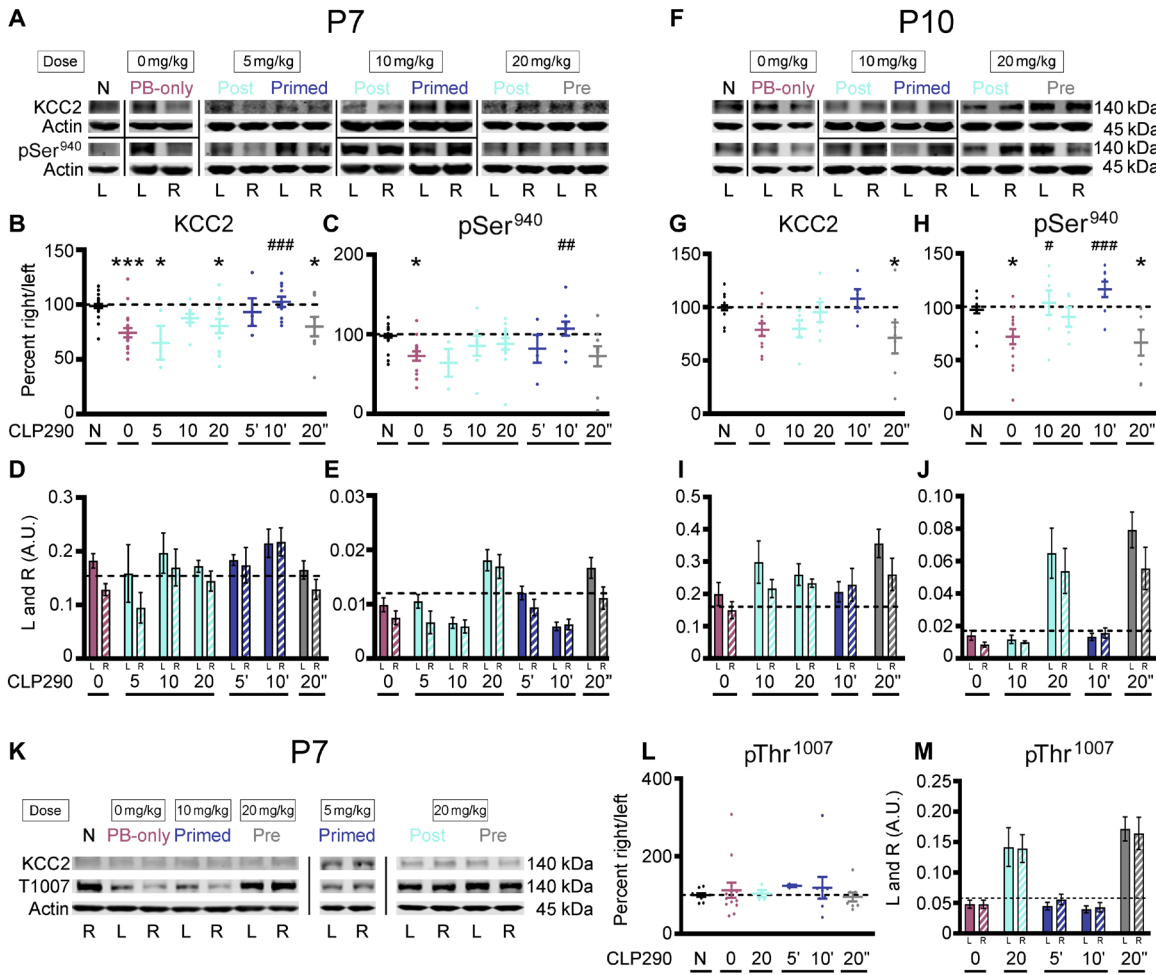


Fig. 6. Effect of CLP290-mediated rescue of refractory seizures on post-ischemic KCC2 down-regulation. (A) Representative Western blots of KCC2 expression and Ser⁹⁴⁰ phosphorylation 24 hours after P7 ischemic seizures. N, naïve. (B) KCC2 and (C) Ser⁹⁴⁰ as percent ipsilateral/contralateral (right/left). (D) KCC2 and (E) Ser⁹⁴⁰ in left ("L") and right ("R") hemispheres. (F) Representative Western blots of KCC2 and Ser⁹⁴⁰ 24 hours after P10 ischemic seizures. (G) KCC2 and (H) Ser⁹⁴⁰ as percent R/L. (I) KCC2 and (J) Ser⁹⁴⁰ in left and right hemispheres. (K) Representative Western blot of KCC2 and Thr¹⁰⁰⁷ 24 hours after ischemic neonatal seizures. (L) Thr¹⁰⁰⁷ phosphorylation as percent R/L. (M) Thr¹⁰⁰⁷ phosphorylation in left and right hemispheres. *P < 0.05 and ***P < 0.001 by one-way ANOVA versus naïve. #P < 0.05, ##P < 0.01, and ###P < 0.001 versus PB-only. P7 pups: naïve, n = 27; PB-only, n = 18; 5 post, n = 3; 10 post, n = 9; 20 post, n = 13; 5', n = 4; 10', n = 11; 20 pre, n = 9 pups. A. U., arbitrary units.

KCC2 functional enhancers must either increase KCC2 surface stability and/or decrease Thr¹⁰⁰⁷ phosphorylation (54, 55). Therefore, Thr¹⁰⁰⁷ phosphorylation was assessed 24 hours after P7 ischemic neonatal seizures (Fig. 6, K to M, and data file S1). Ischemia did not significantly change Thr¹⁰⁰⁷ phosphorylation at 24 hours in either hemisphere (Fig. 6, K to M, and fig. S4B). The 10-min CLP290 dose also did not significantly modulate Thr¹⁰⁰⁷ phosphorylation; however, bolus administration of CLP290 (20 mg/kg) resulted in increased Thr¹⁰⁰⁷ phosphorylation at 24 hours in both 20 mg/kg pre- and posttreatment groups (Fig. 6, K to M, and fig. S4B). Ischemic neonatal seizures at P7 did not significantly modulate the phosphorylation at the Thr¹⁰⁰⁷ residue.

CLP290 rescue of PB-resistant seizures was not mediated through brain-derived neurotrophic factor-TrkB signaling

Ischemic neonatal seizures at P7 induce a robust bilateral increase in TrkB expression and phosphorylation of Tyr⁸¹⁶ (16, 27).

Similarly here, TrkB expression and Tyr⁸¹⁶ phosphorylation were up-regulated bilaterally in the PB-only group 24 hours after ischemic neonatal seizures at P7 (figs. S5, A to E, and S6) but not at P10 (figs. S5, F to J, and S6). The bilateral increase in post-ischemic TrkB expression and Tyr⁸¹⁶ phosphorylation was detected as previously characterized (16). CLP290 had no effect on the global increase in TrkB expression (fig. S5, B and D). Ipsilateral phosphorylation of the Tyr⁸¹⁶ residue was modulated by ischemia at P7 (fig. S5C) and was rescued by CLP290 (fig. S5C). In this model, ischemic neonatal seizures at P10 were PB responsive, and P10 pups did not show activation of TrkB (fig. S5, G to J). These results suggest that the CLP290-mediated seizure suppression in the 10' group at P7 was independent of TrkB.

In vitro CLP257 incubation increases KCC2 membrane insertion

CLP257 has been shown to increase KCC2 membrane expression, restore chloride extrusion capacity, and reduce the duration of

ictal-like discharges in vitro (20, 44). CLP257 and its prodrug CLP290 have been shown to increase KCC2 membrane expression, restore impaired chloride homeostasis, hyperpolarize GABA equilibrium potentials, and improve outcomes in neuropsychiatric mouse models associated with KCC2 hypofunction (20, 50, 51, 56, 57). It has been suggested that the net effect of KCC2 functional enhancement by either CLP257 or CLP290 may emerge from relatively small changes in KCC2 function (10, 20, 58). Further, the neonatal brain tightly regulates KCC2 activity via Ser⁹⁴⁰ and Thr¹⁰⁰⁷ phosphorylation (23), and it is unknown whether age-dependent mechanisms affect KCC2 functional enhancement. Therefore, P7 neonatal brain sections were incubated with graded doses of CLP257 or CLP290 (Fig. 7, A to C). CLP257 (500 μM) significantly increased membrane KCC2 and Ser⁹⁴⁰ phosphorylation (Fig. 7B). Thr¹⁰⁰⁷ phosphorylation at the membrane did not show significant modulation when treated with CLP257 (Fig. 7B). The phosphorylation of Ser⁹⁴⁰ increases KCC2 plasma membrane insertion and transport activity (47, 59). To assess whether the Ser⁹⁴⁰ site was necessary for CLP257-mediated KCC2 membrane insertion, brain sections from S940A^{+/+} knock-in mutant mice (25) were treated with CLP257 (Fig. 7, D to G). Without the ability to phosphorylate Ser⁹⁴⁰, CLP257 failed to increase KCC2 membrane insertion (Fig. 7F).

DISCUSSION

KCC2 is a key regulator of neuronal intracellular chloride (5, 60) and is regulated by diverse mechanisms (10, 11). Acute enhancement of KCC2 membrane stability and function could reestablish synaptic inhibition in seizing neonatal brains when positive GABAR modulators, like PB, fail to curb severe recurrent seizures (14, 61). Documented KCC2 hypofunction, such as in postmortem cerebral samples from preterm infants with white matter injury (62), supports this approach. This acute strategy is distinct from chronic overexpression or enhancement of KCC2 function in neurons with stable endogenous KCC2 expression, which could be detrimental to developing brains (63, 64). Moderate and severe seizures due to hypoxic-ischemic encephalopathy are clinically associated with substantial hourly or daily seizure burdens, which tend to cluster into high-seizing and nonseizing periods (4, 65); however, they are transient in nature. An acute protocol of rescuing KCC2 hypofunction during this critical period would help mitigate both the refractory neonatal seizures and their long-term consequences.

Now, there are very few studies evaluating CLP290 efficacy in models of neurological disease, and there is an urgent need for the discovery of additional KCC2 functional enhancers. The De Koninck group originally identified CLP257 as a KCC2 functional enhancer using high-throughput screening (20). The prodrug CLP290 reportedly has improved pharmacokinetics over CLP257 and rescues neuropathic pain in a rat model, and multiple studies have shown that CLP290 improves outcomes in models of neuropathic pain and spinal cord injury associated with KCC2 hypofunction (20, 51, 57). In vitro studies have proposed that the active drug CLP257 does not directly modulate KCC2 activity but potentiates GABA_AR activity (66, 67). Here, our results demonstrate that phosphorylation of the Ser⁹⁴⁰ residue is necessary for the CLP257-mediated increase in KCC2 expression at the membrane, as well as for the CLP290-mediated antiseizure effect in vivo. These results suggest that the efficacy of CLP290 as a KCC2 functional enhancer is dependent upon the phosphorylation of Ser⁹⁴⁰. The identification

of more efficient KCC2 functional enhancers targeting these phosphorylation sites is needed.

The mechanisms by which CLP290 enhances KCC2 function in neurons are not well understood (20, 66, 67). The ability of CLP290 to rescue both KCC2 expression and Ser⁹⁴⁰ phosphorylation 24 hours after ischemia in this study is similar to those reported with the TrkB antagonist ANA12 (16); however, our findings are also distinct, given that CLP290 had no effect on subduing the ischemia-induced activation of TrkB. Its ability to increase KCC2 membrane insertion in P7 brain sections and its inability to subdue ischemic seizures in the mutant KCC2 S940A^{+/+} pups support its role as a KCC2 functional enhancer acting through its Ser⁹⁴⁰ phosphorylation site. S940A^{+/+} pups not only showed an increase in seizure susceptibility to the P7 ischemic insult, but importantly, we documented the occurrence of spontaneous epileptiform discharges in the naïve mutant pups at P7. S940A^{+/+} pups did not show the age-dependent (P7 versus P10) differences in ischemic seizure susceptibility highlighting the developmental role of Ser⁹⁴⁰ phosphorylation in hyperexcitability of the immature brain. The significance of this finding is highlighted in recent reports of KCC2 mutations in early-onset epileptic syndromes (8), in which mutant KCC2 is associated with a reduction in Ser⁹⁴⁰ phosphorylation (39) and impaired Cl⁻ extrusion (40, 68). The high seizure burdens and early mortality detected in S940A^{+/+} pups and low-seizure susceptibility of the T1007A^{+/+} pups to the repeated dose PTZ challenge at P12 may further support the role of the two sites in the evolution of epileptogenesis after P7 neonatal seizures in the CD-1 model.

KCC2 can autoregulate its Cl⁻ extrusion capacity using positive and negative modulators of its multiple phosphoregulation sites (23). Modest KCC2 hypofunction can play a substantial role in the emergence of neurological disorders (58). For example, KCC2-enhancing compounds rescue neurodevelopmental phenotypes in models of Rett syndrome (69), suggesting that genetic strategies to increase KCC2 expression should be compared to functional enhancers like CLP290 in future studies. Overexpression of KCC2 in neurons may not only be detrimental but may also trigger endogenous, negative-feedback homeostatic pathways. Notably, pushing KCC2 function beyond its physiological levels is reportedly difficult in simulation studies (10). The marked reduction in baseline seizure susceptibility and the up-regulation of Thr¹⁰⁰⁷ phosphorylation observed here in P7 mice after treatment with the higher-dose (20 mg/kg) CLP290—in contrast to the responses at lower doses and in untreated mice—could suggest such a compensatory homeostatic mechanism of KCC2 activation by CLP290. The results here for CLP257-mediated Thr¹⁰⁰⁷ phosphorylation in vitro versus in vivo may indicate a temporal regulation of the homeostatic response but needs further investigation.

Studies have shown that, during induced status epilepticus, reduced Cl⁻ extrusion capacity and exacerbated activity-dependent Cl⁻ loading can result in GABAergic transmission being ictogenic (meaning to generate a seizure) (13). Optogenetic stimulation of GABAergic interneurons in this status, epilepticus-like state, enhances the epileptiform activity in a GABA_AR-dependent manner (70), indicating GABA-mediated depolarization. These findings support data both from our model and clinical reports wherein after an initial loading dose of PB fails to curb seizures, additional PB doses do not help rescue the refractoriness (2, 71). In addition, given the toxicity of high-dose PB on neonatal brains, such protocols may be counterproductive in both the short and long terms (72–74).

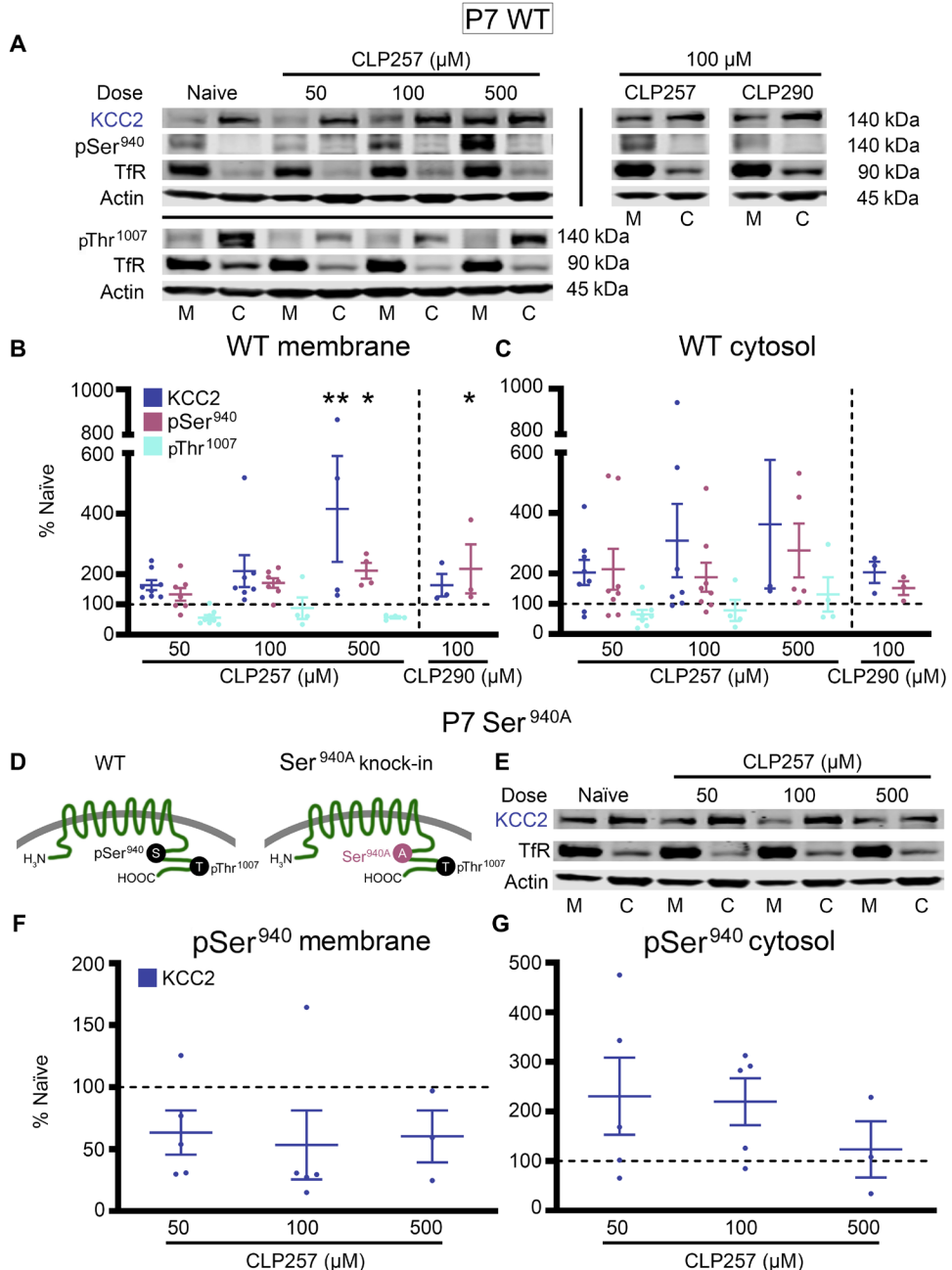


Fig. 7. In vitro CLP257 treatment up-regulated membrane KCC2 expression and Ser⁹⁴⁰ phosphorylation. (A) KCC2, Ser⁹⁴⁰, and Thr¹⁰⁰⁷ in the plasma membrane (M) and cytosol (C) for all treated P7 wild-type (WT) brain slices. (B) KCC2, Ser⁹⁴⁰, and Thr¹⁰⁰⁷ in the membrane and (C) cytosol for all treatment groups plotted as percent of naïve. Number of WT P7 pups: $n = 8$ (50 μ M CLP257), $n = 7$ (100 μ M CLP257), $n = 4$ (500 μ M CLP257), and $n = 3$ (100 μ M CLP290). (D) Graphical representation of S940A^{+/+} knock-in mutant mice (25). (E to G) Western blotting for KCC2 expression in the plasma membrane and cytosol for all S940A^{+/+} P7 pups (E). Quantified KCC2 expression in the membrane (F) and cytosol (G) for all S940A^{+/+} treatment groups plotted as percent of naïve. All proteins of interest in the cytosol were normalized to housekeeping protein β -actin; all proteins of interest in the plasma membrane were normalized to transferrin (TfR); and phosphoproteins were normalized to their respective total protein. Data plots show all data points with means \pm SEM. * $P < 0.05$ and ** $P < 0.01$ by one-way ANOVA. S940A^{+/+} P7 pups: $n = 5$ (50 μ M CLP257), $n = 5$ (100 μ M CLP257), and $n = 3$ (500 μ M CLP257).

KCC2 hypofunction is emerging as a substantial cause of impaired inhibitory neurotransmission underlying multiple neurological disorders (5, 48, 61). Notably, research into both refractory seizures and refractory spinal nerve pain has identified KCC2 hypofunction as a common underlying cause. Future studies should investigate chloride extrusion-dependent and chloride extrusion-independent functions of KCC2 in neurological disease. In this study, we have shown that enhancing KCC2 function in a well-characterized preclinical model of refractory seizures can not only rescue the acute PB refractoriness but also help mitigate epileptogenesis with early intervention. Our findings highlight the role of KCC2 hypofunction and its phosphoregulation in hypoxic-ischemic encephalopathy-related refractory seizures (Fig. 8) and support the application and development of KCC2 enhancers specifically for the neonatal period.

MATERIALS AND METHODS

Experimental paradigm and reagents

In CLP290 and CLP257 experiments, all pups (P7 and P10, regardless of treatment group) received a loading dose of PB (25 mg/kg) dissolved in 100% isotonic phosphate-buffered saline (PBS) delivered by intraperitoneal injection at 1 hour. All injections were administered using Hamilton syringes, and all drugs were prepared the day of the experiments. CLP290 and CLP257 were both dissolved in 45/55% 2-hydroxypropyl- β -cyclodextrin/PBS with a pH between 7.2 and 7.5. Pups were assigned to the PB-only, post-, primed, or pretreatment groups (Fig. 1). PB-only treatment is defined by the single administration of the PB (25 mg/kg) at 1 hour after unilateral carotid ligation without further intervention. Posttreatment (post) is defined by intraperitoneal administration of CLP290 (5, 10, or 20 mg/kg; labeled 5', 10', or 20' in the figures) immediately after unilateral carotid ligation and PB administration at 1 hour. Primed treatment is defined by the administration of CLP290 (5, 10, or 20 mg/kg; labeled 5', 10', or 20' in the figures) 4 hours preceding unilateral carotid ligation and another injection

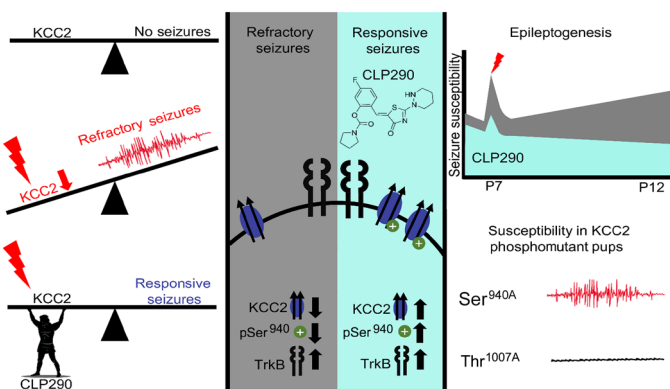


Fig. 8. Summary. Targeting ischemia-induced KCC2 hypofunction with the KCC2 functional enhancer CLP290 rescued refractory neonatal seizures at P7 and mitigated epileptogenesis in same pups at P12.

of the same dose immediately after unilateral carotid ligation with PB at 1 hour. Pretreatment is defined by the single administration of CLP290 (20 mg/kg; labeled 20" in the figures) 4 hours before unilateral carotid ligation with PB at 1 hour after ligation. In experiments assessing CLP290 versus CLP257, P7 pups were administered CLP257 (10 mg/kg) in a primed treatment group with PB at 1 hour after unilateral carotid ligation. For convenience, reagents are tabulated in the Supplementary Materials (table S1).

Animals

All experimental procedures and protocols were conducted in compliance with guidelines by the Committee on the Ethics of Animal Experiments (permit number: A3272-01) and were approved by the Animal Care and Use of Committee of Johns Hopkins University. CD1 litters were purchased from Charles River Laboratories (Wilmington, MA.). Newly born CD-1 litters ($n = 10$) were delivered with a dam at P3 or P4 and allowed to acclimate. S940A^{+/+} and T906A/T1007A^{+/+} mice were a gift from the laboratory of S. J. Moss at Tufts University School of Medicine. Equivalent numbers of male and female pups were introduced into the study. All mice were housed on a 12-hour light/12-hour dark cycle with food and water provided ad libitum.

Unilateral carotid ligation

A comprehensive protocol for unilateral carotid ligation and neonatal video-EEG recordings has been published (75). At P7 or P10, animals were subjected to permanent unilateral ligation (without transection) of the right common carotid artery using 6-0 Surgisilk (Fine Science Tools, BC Canada) under isoflurane anesthesia. The outer skin was closed with 6-0 monofilament nylon (Covidien, MA), and lidocaine was applied as local anesthetic. Animals were implanted with three subdermal EEG scalp electrodes: 1 recording and 1 reference overlying the bilateral parietal cortices and 1 ground electrode overlying the rostrum. Wire electrodes (IVES EEG; model #SWE-L25-MA, IVES EEG Solutions, USA) were implanted subdermally and fixed in position with cyanoacrylate adhesive (KrazyGlue). Pups recovered from anesthesia over a few minutes. Animals were tethered to a preamplifier within a recording chamber for 2 hours of continuous vEEG recording and were maintained at 36°C with heated isothermal pads. At the end of the recording session, subdermal electrodes were removed, and the pups were returned to the dam.

In vivo vEEG recording and analyses

EEG recordings were acquired using Sirenia Acquisition software with synchronous video capture (Pinnacle Technology Inc.). Data acquisition was done with sampling rates of 400 Hz that had a preamplifier gain of 100 and the filters of 0.5-Hz high pass and 50-Hz low pass. The data were scored by binning EEG in 10s epochs. Similar to our previous studies (15), seizures were defined as electrographic ictal events that consisted of rhythmic spikes of high amplitude and diffuse peak frequency of ≥ 7 to 8 Hz (meaning peak frequency detected by automated spectral power analysis) lasting ≥ 6 s (meaning longer than half of each 10s epoch). Short-duration burst activity lasting < 6 s (brief runs of epileptiform discharges) was not included for seizure burden calculations, as in previous studies with the model. Mean time spent seizing for first hour baseline seizure burden compared to the second hour post-PB seizure burden was quantified in seconds. Mean seizure suppression was calculated using Eq. 1

$$\% \text{Seizure suppression} =$$

$$\frac{(1\text{st hour seizure burden} - 2\text{nd hour seizure burden})}{(1\text{st hour seizure burden})} * 100 \quad (1)$$

Mean ictal events and ictal durations (seconds per event) were calculated for first versus second hour.

CLP290 plasma and brain availability in neonatal mice

Standards for HPLC were created using CLP257 (MilliporeSigma, USA) and CLP290 (Yves De Koninck Lab). P7 and P10 naïve pups of both sexes were administered CLP290 intraperitoneally as three treatment groups: 10, 20 mg/kg, or vehicle. After 4 hours, pups were anesthetized with chloral hydrate (90 mg/ml; i.p.), and transcardiac blood samples (100 μ l) were collected. The same pups were transcardially perfused with ice-cold PBS, and the whole fresh brains were harvested. Brain samples were flash-frozen in dry ice, homogenized using a sonicator, and stored at -80°C . Blood and brain samples from CLP290-treated and naïve pups were analyzed for CLP290 and CLP257 concentrations via HPLC using a C18 column and 10/90 organic/aqueous mobile phase.

VU0463271

To assess the role of KCC2 inhibition in neonatal seizure severity at P7 after ligation, the potent and selective KCC2 inhibitor VU was administered at 1 hour (0.5 mg/kg; i.p.) in lieu of PB (Fig. 1). VU was dissolved in 20/80% dimethyl sulfoxide/PBS solution. To assess the role of KCC2 antagonism in neonatal seizure occurrence, naïve P7 or P10 pups underwent vEEG with VU (0.25 mg/kg) administered at the start of recording in lieu of ligation and VU (0.5 mg/kg) administered at 1 hour in lieu of PB.

P12 PTZ challenge

To investigate the long-term effects of CLP290 treatment, P12 pups underwent a 3-hour vEEG recording during a challenge with PTZ (dissolved in 100% PBS). At P7, pups were either naïve, PB-only, or P7 CLP290 10'. These P7 pups then underwent a PTZ challenge at P12. All pups were administered PTZ at the beginning of the vEEG recording (20 mg/kg; i.p.), at 1 hour (20 mg/kg; i.p.), and at 2 hours (40 mg/kg; i.p.).

P12 to P15 slice preparation

Coronal brain slices were prepared from CD-1 mice at P12 to P15 that underwent either naïve or PB-only treatment at P7. Pups were deeply anesthetized with isoflurane inhalation and decapitated. The brain was rapidly dissected out and immersed in ice-cold oxygenated cutting solution containing 125 mM NaCl, 3 mM KCl, 1.25 mM NaH₂PO₄, 25 mM NaHCO₃, 0.25 mM CaCl₂, 10 mM MgSO₄, and 11 mM glucose. After 1 to 2 min, the brain was glued onto the platform of a specimen syringe and embedded with 1.6% low-melting point agarose (type I-B), quickly chilled, and transferred into a buffer tank filled with cutting solution. Coronal slices (350 µm) were cut using a VF-300 microtome (Precisionary Instruments Inc., Greenville, NC) and separated from the embedding agarose. Slices were kept in oxygenated holding solution containing 125 mM NaCl, 3 mM KCl, 1.25 mM NaH₂PO₄, 25 mM NaHCO₃, 0.5 mM CaCl₂, 5 mM MgSO₄, and 11 mM glucose, at 34°C for 45 min and thereafter at room temperature.

Field potential recordings

Extracellular field-potential recordings were conducted from layer II/III of the anterior (before hippocampus) and posterior (with hippocampus) cortices, referring to roughly plate 20 and plate 50 in the Paxinos and Watson mouse brain atlas, respectively. Low-resistance glass pipettes (1 to 3 megohm) filled with ACSF were used to record field potentials. A concentric bipolar stimulating electrode (FHC, Bowdoin, ME) was placed in “off-column” areas of layer IV (i.e., ~100 µm lateral to the hypothetical perpendicular line across the recording site) to deliver synaptic stimulation, through a stimulus generator (STG 4002, Multichannel Systems, MCS GmbH, Reutlingen, Germany). The threshold stimulation (T) was determined by the minimal current intensity to evoke a synaptic response. The input-out responses from 1T to 6T were first performed in ACSF and repeated 10 min after bath application of low concentration (1 µM) of GABAzine. Field potentials were recorded in nonclamp mode ($I = 0$) at a high gain ($\alpha = 100$), acquired at 10 kHz, low pass-filtered at 2 kHz, and analyzed offline using the clampfit software (Molecular Devices, Sunnyvale, CA). All chemicals used in this study were purchased from Sigma-Aldrich (St. Louis, MO).

Western blot analysis at 24 hours after ligation

All animals for immunochemical characterizations were anesthetized with chloral hydrate (90 mg/ml; i.p.) before being transcardially perfused with ice-cold saline. The whole fresh brains were removed, the cerebellum was discarded, and the left and right hemispheres were separated. Naïve CLP290 10'-treated mice (fig. S3) were harvested at 4 hours and underwent further microdissection after perfusion to isolate cortex. Brains were stored at -80°C in preparation for further processing. Brain tissue homogenates were made and suspended in tissue protein extraction reagent (TPER) cell lysis buffer containing 10% protease/phosphatase inhibitor cocktail. Total protein amounts were measured using the Bradford protein assay (Bio-Rad, Hercules, CA, USA) at 570 nm, and the samples were diluted in 5× loading buffer for a concentration of 50 µg of protein in 20 µl. Twenty microliters of protein samples was run on 4 to 20% gradient tris-glycine gels (Invitrogen, Gand Island, NY, USA) for 120 min at 130 V and were transferred onto nitrocellulose membranes overnight at 20 V. After the transfer, the nitrocellulose membranes underwent a 1-hour blocking step in Rockland buffer before 6-hour incubation with primary antibodies [for all antibody Research Resource identifiers (RRIDS), see table S1]: mouse α-KCC2 (1:1000; Millipore),

rabbit α-phospho-KCC2-S940 (1:1000; Aviva Systems Biology), rabbit α-phospho-KCC2-T1007 (1:1000; Phospho Solutions) mouse α-TrkB (1:1000; BD Biosciences), rabbit α-phospho-TrkB-Y816 (1:500; Millipore), and mouse α-actin (1:10,000; LI-COR Biosciences). Antibodies were validated as previously described (27). Membranes were then incubated with fluorescent secondary antibodies (1:5000; goat α-rabbit and goat α-mouse, LI-COR Biosciences, USA). Chemiluminescent protein bands were analyzed using the Odyssey infrared imaging system 2.1 (LI-COR Biosciences). The optical density of each protein sample was normalized to their corresponding actin bands run on each lane for internal control. Mean-normalized protein expression levels were then calculated for respective left and right hemispheres. The expression levels of the proteins of interest in ipsilateral hemispheres were normalized to the same in contralateral hemispheres for each pup to examine hemispheric percent change of protein expression.

Surface protein separation

One-millimeter coronal brain slices were obtained from P7 CD-1 mice and recovered for 45 min at 34°C with oxygenation (95%/5% O₂/CO₂). After recovery, slices were incubated with CLP290 or CLP257 at 34°C with oxygenation for 40 min. Slices were placed in TPER cell lysing buffer with Halt protease and phosphatase inhibitors and homogenized via sonication. After 30-min incubation on ice, protein lysates were ultracentrifuged at 210,000g (TLA-120.2 rotor, Beckman Coulter Life Sciences), and supernatants were collected as the cytosolic components. Pellets were resuspended in TPER/HALT buffer and ultracentrifuged; the supernatant was discarded as wash fraction. Pellets were resuspended in TPER/HALT buffer and collected as the membrane components. Membrane and cytosolic components underwent Bradford analysis and Western blotting for protein quantification. Plasma membrane proteins were normalized to transferrin (TfR). Cytosolic proteins were normalized to β-actin.

Statistical analysis

For all experiments, the quantification and analysis of data were performed blinded to the genotype, sex, and treatment conditions. All statistical tests were performed using GraphPad Prism software. Two-way analysis of variance (ANOVA) was performed with Tukey's post hoc correction. One-way ANOVA was performed with Dunnett's post hoc correction. Paired and unpaired *t* tests were two-tailed. Survival analysis was performed by a Mantel-Cox test. Data are represented as bar graphs representing the mean, with dot plots representing each individual data point. Errors bars are ±1 SEM. *P* ≤ 0.05 is reported by threshold, marked with asterisks and hashes that are defined in the legends.

SUPPLEMENTARY MATERIALS

www.science.org/doi/10.1126/scisignal.abg2648

Figs. S1 to S6

Table S1

Data file S1

[View/request a protocol for this paper from Bio-protocol.](https://bio-protocol.org/View/request_a_protocol_for_this_paper_from_Bio-protocol)

REFERENCES AND NOTES

- J. Volpe, T. Inder, B. Darras, L. de Vries, A. du Plessis, J. Neill, J. Perlman, *Volpe's Neurology of the Newborn* (Elsevier, ed. 6, 2017).
- R. Sankar, M. J. Painter, Neonatal seizures: After all these years we still love what doesn't work. *Neurology* **64**, 776–777 (2005).

3. H. C. Glass, J. S. Soul, C. J. Chu, S. L. Massey, C. J. Wusthoff, T. Chang, M. R. Cilio, S. L. Bonifacio, N. S. Abend, C. Thomas, M. Lemmon, C. E. McCulloch, R. A. Shellhaas, Response to antiseizure medications in neonates with acute symptomatic seizures. *Epilepsia* **60**, e20–e24 (2019).
4. G. B. Boylan, N. J. Stevenson, S. Vanhatalo, Monitoring neonatal seizures. *Semin. Fetal Neonatal Med.* **18**, 202–208 (2013).
5. K. Kaila, T. J. Price, J. A. Payne, M. Puskarjov, J. Voipio, Cation-chloride cotransporters in neuronal development, plasticity and disease. *Nat. Rev. Neurosci.* **15**, 637–654 (2014).
6. G. Sedmak, N. Jovanović-Milošević, M. Puskarjov, M. Ulamec, B. Krušlin, K. Kaila, M. Judaš, Developmental expression patterns of KCC2 and functionally associated molecules in the human brain. *Cereb. Cortex* **26**, 4574–4589 (2016).
7. Y. Ben-Ari, Excitatory actions of GABA during development: The nature of the nurture. *Nat. Rev. Neurosci.* **3**, 728–739 (2002).
8. P. Q. Duy, W. B. David, K. T. Kahle, Identification of KCC2 Mutations in human epilepsy suggests strategies for therapeutic transporter modulation. *Front. Cell. Neurosci.* **13**, 515 (2019).
9. J. A. French, Refractory epilepsy: Clinical overview. *Epilepsia* **48**, 3–7 (2007).
10. N. Doyon, L. Vinay, S. A. Prescott, Y. De Koninck, Chloride regulation: A dynamic equilibrium crucial for synaptic inhibition. *Neuron* **89**, 1157–1172 (2016).
11. B. J. Sullivan, S. D. Kadam, in *Neuronal Chloride Transporters in Health and Disease*, X. Tang, Ed. (Elsevier, ed. 1, 2020), p. 650.
12. R. Nardou, S. Yamamoto, G. Chazal, A. Bhar, N. Ferrand, O. Dulac, Y. Ben-Ari, I. Khalilov, Neuronal chloride accumulation and excitatory GABA underlie aggravation of neonatal epileptiform activities by phenobarbital. *Brain J. Neurol.* **134**, 987–1002 (2011).
13. R. J. Burman, J. S. Selfe, J. H. Lee, M. van den Berg, A. Calin, N. Kodadu, R. Wright, S. E. Newey, R. R. Parrish, A. A. Katz, J. M. Wilmsurst, C. J. Akerman, A. J. Trevelyan, J. V. Raimondo, Excitatory GABAergic signalling is associated with benzodiazepine resistance in status epilepticus. *Brain J. Neurol.* **142**, 3482–3501 (2019).
14. S. K. Kang, G. J. Markowitz, S. T. Kim, M. V. Johnston, S. D. Kadam, Age- and sex-dependent susceptibility to phenobarbital-resistant neonatal seizures: Role of chloride co-transporters. *Front. Cell. Neurosci.* **9**, 173 (2015).
15. S. K. Kang, M. V. Johnston, S. D. Kadam, Acute TrkB inhibition rescues phenobarbital-resistant seizures in a mouse model of neonatal ischemia. *Eur. J. Neurosci.* **42**, 2792–2804 (2015).
16. B. M. Carter, B. J. Sullivan, J. R. Landers, S. D. Kadam, Dose-dependent reversal of KCC2 hypofunction and phenobarbital-resistant neonatal seizures by ANA12. *Sci. Rep.* **8**, 11987 (2018).
17. S. K. Kang, S. Ammanuel, S. Thodupunuri, D. A. Adler, M. V. Johnston, S. D. Kadam, Sleep dysfunction following neonatal ischemic seizures are differential by neonatal age of insult as determined by qEEG in a mouse model. *Neurobiol. Dis.* **116**, 1–12 (2018).
18. S. K. Kang, S. Ammanuel, D. A. Adler, S. D. Kadam, Rescue of PB-resistant neonatal seizures with single-dose of small-molecule TrkB antagonist show long-term benefits. *Epilepsy Res.* **159**, 106249 (2020).
19. B. J. Sullivan, S. D. Kadam, Brain-derived neurotrophic factor in neonatal seizures. *Pediatr. Neurol.* **118**, 35–39 (2021).
20. M. Gagnon, M. J. Bergeron, G. Lavertu, A. Castonguay, S. Tripathy, R. P. Bonin, J. Perez-Sanchez, D. Boudreau, B. Wang, L. Dumas, I. Valade, K. Bachand, M. Jacob-Wagner, C. Tardif, I. Kianicka, P. Isenring, G. Attardo, J. A. M. Coull, Y. De Koninck, Chloride extrusion enhancers as novel therapeutics for neurological diseases. *Nat. Med.* **19**, 1524–1528 (2013).
21. H. C. Glass, Z. M. Grinspan, R. A. Shellhaas, Outcomes after acute symptomatic seizures in neonates. *Semin. Fetal Neonatal Med.* **23**, 218–222 (2018).
22. S. K. Kang, S. D. Kadam, Neonatal seizures: Impact on neurodevelopmental outcomes. *Front. Pediatr.* **3**, 101 (2015).
23. Y. E. Moore, L. C. Conway, N. J. Brandon, T. Z. Deeb, S. J. Moss, Developmental regulation of KCC2 phosphorylation has long-term impacts on cognitive function. *Front. Mol. Neurosci.* **12**, 173 (2019).
24. Y. E. Moore, T. Z. Deeb, H. Chadchankar, N. J. Brandon, S. J. Moss, Potentiating KCC2 activity is sufficient to limit the onset and severity of seizures. *Proc. Natl. Acad. Sci.* **115**, 10166–10171 (2018).
25. L. Silayeva, T. Z. Deeb, R. M. Hines, M. R. Kelley, M. B. Munoz, H. H. C. Lee, N. J. Brandon, J. Dunlop, J. Maguire, P. A. Davies, S. J. Moss, KCC2 activity is critical in limiting the onset and severity of status epilepticus. *Proc. Natl. Acad. Sci. U.S.A.* **112**, 3523–3528 (2015).
26. M. Watanabe, J. Zhang, M. S. Mansuri, J. Duan, J. K. Karimy, E. Delpire, S. L. Alper, R. P. Lifton, A. Fukuda, K. T. Kahle, Developmentally regulated KCC2 phosphorylation is essential for dynamic GABA-mediated inhibition and survival. *Sci. Signal.* **12**, eaaw9315 (2019).
27. P. A. Kipnis, B. J. Sullivan, B. M. Carter, S. D. Kadam, TrkB agonists prevent postischemic emergence of refractory neonatal seizures in mice. *JCI Insight* **5**, e136007 (2020).
28. S. C. Kharod, S. K. Kang, S. D. Kadam, Off-label use of bumetanide for brain disorders: An overview. *Front. Neurosci.* **13**, 310 (2019).
29. M. Puskarjov, K. T. Kahle, E. Ruusuvuori, K. Kaila, Pharmacotherapeutic targeting of cation-chloride cotransporters in neonatal seizures. *Epilepsia* **55**, 806–818 (2014).
30. C. P. Panayiotopoulos, *Neonatal Seizures and Neonatal Syndromes* (Bladon Medical Publishing, 2005).
31. E. Kossoff, Neonatal seizures due to hypoxic-ischemic encephalopathy: Should we care? *Epilepsy Curr.* **11**, 147–148 (2011).
32. S. C. Kharod, B. M. Carter, S. D. Kadam, Pharmaco-resistant neonatal seizures: Critical mechanistic insights from a chemoconvulsant model. *Dev. Neurobiol.* **78**, 1117–1130 (2018).
33. S. D. Kadam, F. E. Dudek, Temporal progression of evoked field potentials in neocortical slices after unilateral hypoxia-ischemia in perinatal rats: Correlation with cortical epileptogenesis. *Neuroscience* **316**, 232–248 (2016).
34. R. F. Hunt, S. W. Scheff, B. N. Smith, Posttraumatic epilepsy after controlled cortical impact injury in mice. *Exp. Neurol.* **215**, 243–252 (2009).
35. T. P. Sutula, F. E. Dudek, Unmasking recurrent excitation generated by mossy fiber sprouting in the epileptic dentate gyrus: An emergent property of a complex system. *Prog. Brain Res.* **163**, 541–563 (2007).
36. J.-P. Wuarin, F. E. Dudek, Electrographic seizures and new recurrent excitatory circuits in the dentate gyrus of hippocampal slices from kainate-treated epileptic rats. *J. Neurosci.* **16**, 4438–4448 (1996).
37. N.-S. Woo, J. Lu, R. England, R. McClellan, S. Dufour, D. B. Mount, A. Y. Deutch, D. M. Lovinger, E. Delpire, Hyperexcitability and epilepsy associated with disruption of the mouse neuronal-specific K-Cl cotransporter gene. *Hippocampus* **12**, 258–268 (2002).
38. C. A. Hubner, Disruption of KCC2 reveals an essential role of K-Cl cotransport already in early synaptic inhibition. *Neuron* **30**, 515–524 (2001).
39. K. T. Kahle, N. D. Merner, P. Friedel, L. Silayeva, B. Liang, A. Khanna, Y. Shang, P. Lachance-Touchette, C. Bourassa, A. Levert, P. A. Dion, B. Walcott, D. Spiegelman, A. Dionne-Laporte, A. Hodgkinson, P. Awadalla, H. Nikbakht, J. Majewski, P. Cossette, T. Z. Deeb, S. J. Moss, I. Medina, G. A. Rouleau, Genetically encoded impairment of neuronal KCC2 cotransporter function in human idiopathic generalized epilepsy. *EMBO Rep.* **15**, 766–774 (2014).
40. M. Puskarjov, P. Seja, S. E. Heron, T. C. Williams, F. Ahmad, X. Iona, K. L. Oliver, B. E. Grinton, L. Vutskits, I. E. Scheffer, S. Petrou, P. Blaeser, L. M. Dibbens, S. F. Berkovic, K. Kaila, A variant of KCC2 from patients with febrile seizures impairs neuronal Cl⁻ extrusion and dendritic spine formation. *EMBO Rep.* **15**, 723–729 (2014).
41. L. I. Pisella, J.-L. Gaiarsa, D. Diabira, J. Zhang, I. Khalilov, J. Duan, K. T. Kahle, I. Medina, Impaired regulation of KCC2 phosphorylation leads to neuronal network dysfunction and neurodevelopmental pathology. *Sci. Signal.* **12**, eaay0300 (2019).
42. L. Nashef, E. L. So, P. Ryvlin, T. Tomson, Unifying the definitions of sudden unexpected death in epilepsy. *Epilepsia* **53**, 227–233 (2012).
43. S. Sivakumaran, R. A. Cardarelli, J. Maguire, M. R. Kelley, L. Silayeva, D. H. Morrow, J. Mukherjee, Y. E. Moore, R. J. Mather, M. E. Duggan, N. J. Brandon, J. Dunlop, S. Zicha, S. J. Moss, T. Z. Deeb, Selective inhibition of KCC2 leads to hyperexcitability and epileptiform discharges in hippocampal slices and in vivo. *J. Neurosci.* **35**, 8291–8296 (2015).
44. V. I. Dzhala, K. J. Staley, KCC2 chloride transport contributes to the termination of ictal epileptiform activity. *eNeuro* **8**, ENEURO.0208-20.2020 (2020).
45. C. Rivera, J. Voipio, J. Thomas-Crusells, H. Li, Z. Emri, S. Sipilä, J. A. Payne, L. Minichiello, M. Saarma, K. Kaila, Mechanism of activity-dependent downregulation of the neuron-specific K-Cl cotransporter KCC2. *J. Neurosci.* **24**, 4683–4691 (2004).
46. H. R. Pathak, F. Weissinger, M. Terunuma, G. C. Carlson, F.-C. Hsu, S. J. Moss, D. A. Coulter, Disrupted dentate granule cell chloride regulation enhances synaptic excitability during development of temporal lobe epilepsy. *J. Neurosci.* **27**, 14012–14022 (2007).
47. H. H. Lee, T. Z. Deeb, J. A. Walker, P. A. Davies, S. J. Moss, NMDA receptor activity downregulates KCC2 resulting in depolarizing GABA_A receptor-mediated currents. *Nat. Neurosci.* **14**, 736–743 (2011).
48. G. Barashchenko, S. Heft, A. Aertsens, T. Kirschstein, R. Köhling, Positive shifts of the GABA_A receptor reversal potential due to altered chloride homeostasis is widespread after status epilepticus. *Epilepsia* **52**, 1570–1578 (2011).
49. T. Akita, A. Fukuda, Intracellular Cl⁻ dysregulation causing and caused by pathogenic neuronal activity. *Pflügers Arch. Eur. J. Physiol.* **472**, 977–987 (2020).
50. P. N. Lizhnyak, P. P. Muldoon, P. P. Pilaka, J. Povlishock, A. K. Ottens, Traumatic brain injury temporal proteome guides KCC2-targeted therapy. *J. Neurotrauma* **36**, 3092–3102 (2019).
51. B. Chen, Y. Li, B. Yu, Z. Zhang, B. Brommer, P. R. Williams, Y. Liu, S. V. Hegarty, S. Zhou, J. Zhu, H. Guo, Y. Lu, Y. Zhang, X. Gu, Z. He, Reactivation of dormant relay pathways in injured spinal cord by KCC2 manipulations. *Cell* **174**, 521–535.e13 (2018).
52. J. Rinehart, Y. D. Maksimova, J. E. Tanis, K. L. Stone, C. A. Hodson, J. Zhang, M. Risinger, W. Pan, D. Wu, C. M. Colangelo, B. Forbush, C. H. Joiner, E. E. Gulcicek, P. G. Gallagher, R. P. Lifton, Sites of regulated phosphorylation that control K-Cl cotransporter activity. *Cell* **138**, 525–536 (2009).

53. S. Titz, E. M. Sammler, S. G. Hormuzdi, Could tuning of the inhibitory tone involve graded changes in neuronal chloride transport? *Neuropharmacology* **95**, 321–331 (2015).
54. L. C. Conway, R. A. Cardarelli, Y. E. Moore, K. Jones, L. J. McWilliams, D. J. Baker, M. P. Burnham, R. W. Bürl, Q. Wang, N. J. Brandon, S. J. Moss, T. Z. Deeb, N-Ethylmaleimide increases KCC2 cotransporter activity by modulating transporter phosphorylation. *J. Biol. Chem.* **292**, 21253–21263 (2017).
55. Y. E. Moore, M. R. Kelley, N. J. Brandon, T. Z. Deeb, S. J. Moss, Seizing control of KCC2: A new therapeutic target for epilepsy. *Trends Neurosci.* **40**, 555–571 (2017).
56. F. Ferrini, L.-E. Lorenzo, A. G. Godin, M. L. Quang, Y. De Koninck, Enhancing KCC2 function counteracts morphine-induced hyperalgesia. *Sci. Rep.* **7**, 3870 (2017).
57. J. C. S. Mapplebeck, L.-E. Lorenzo, K. Y. Lee, C. Gauthier, M. M. Muley, Y. De Koninck, S. A. Prescott, M. W. Salter, Chloride dysregulation through downregulation of KCC2 mediates neuropathic pain in both sexes. *Cell Rep.* **28**, 590–596.e4 (2019).
58. N. Doyon, S. A. Prescott, Y. De Koninck, Mild KCC2 hypofunction causes inconspicuous chloride dysregulation that degrades neural coding. *Front. Cell. Neurosci.* **9**, 516 (2016).
59. H. H. C. Lee, J. A. Walker, J. R. Williams, R. J. Goodier, J. A. Payne, S. J. Moss, Direct protein kinase C-dependent phosphorylation regulates the cell surface stability and activity of the potassium chloride cotransporter KCC2. *J. Biol. Chem.* **282**, 29777–29784 (2007).
60. G. Gamba, Molecular physiology and pathophysiology of electroneutral cation-chloride cotransporters. *Physiol. Rev.* **85**, 423–493 (2005).
61. M. Johne, K. Römermann, P. Hampel, B. Gailus, W. Theilmann, T. Ala-Kurikka, K. Kaila, W. Löscher, Phenobarbital and midazolam suppress neonatal seizures in a noninvasive rat model of birth asphyxia, whereas bumetanide is ineffective. *Epilepsia* **62**, 920–934 (2021).
62. S. Robinson, I. Mikolaenko, I. Thompson, M. L. Cohen, M. Goyal, Loss of cation-chloride cotransporter expression in preterm infants with white matter lesions: Implications for the pathogenesis of epilepsy. *J. Neuropathol. Exp. Neurol.* **69**, 565–572 (2010).
63. K. T. Kahle, K. J. Staley, B. V. Nahed, G. Gamba, S. C. Hebert, R. P. Lifton, D. B. Mount, Roles of the cation-chloride cotransporters in neurological disease. *Nat. Clin. Pract. Neurol.* **4**, 490–503 (2008).
64. S. Hamidi, M. Avoli, KCC2 function modulates in vitro ictogenesis. *Neurobiol. Dis.* **79**, 51–58 (2015).
65. G. B. Boylan, R. M. Pressler, Neonatal seizures: The journey so far. *Semin. Fetal Neonatal Med.* **18**, 173–174 (2013).
66. R. A. Cardarelli, K. Jones, L. I. Pisella, H. J. Wobst, L. J. McWilliams, P. M. Sharpe, M. P. Burnham, D. J. Baker, I. Chudotvorova, J. Guyot, L. Silayeva, D. H. Morrow, N. Dekker, S. Zicha, P. A. Davies, J. Holenz, M. E. Duggan, J. Dunlop, R. J. Mather, Q. Wang, I. Medina, N. J. Brandon, T. Z. Deeb, S. J. Moss, The small molecule CLP257 does not modify activity of the K⁺-Cl⁻ co-transporter KCC2 but does potentiate GABA_A receptor activity. *Nat. Med.* **23**, 1394–1396 (2017).
67. M. Gagnon, M. J. Bergeron, J. Perez-Sánchez, I. Plasencia-Fernández, L.-E. Lorenzo, A. G. Godin, A. Castonguay, R. P. Bonin, Y. De Koninck, Reply to The small molecule CLP257 does not modify activity of the K⁺-Cl⁻ co-transporter KCC2 but does potentiate GABA_A receptor activity. *Nat. Med.* **23**, 1396–1398 (2017).
68. H. Saitsu, M. Watanabe, T. Akita, C. Ohba, K. Sugai, W. P. Ong, H. Shiraishi, S. Yuasa, H. Matsumoto, K. T. Beng, S. Saitoh, S. Miyatake, M. Nakashima, N. Miyake, M. Kato, A. Fukuda, N. Matsumoto, Impaired neuronal KCC2 function by biallelic SLC12A5 mutations in migrating focal seizures and severe developmental delay. *Sci. Rep.* **6**, 30072 (2016).
69. X. Tang, J. Drotar, K. Li, C. D. Clairmont, A. S. Brumm, A. J. Sullins, H. Wu, X. S. Liu, J. Wang, N. S. Gray, M. Sur, R. Jaenisch, Pharmacological enhancement of KCC2 gene expression exerts therapeutic effects on human Rett syndrome neurons and Mecp2 mutant mice. *Sci. Transl. Med.* **11**, eaau0164 (2019).
70. V. Magloire, J. Cornford, A. Lieb, D. M. Kullmann, I. Pavlov, KCC2 overexpression prevents the paradoxical seizure-promoting action of somatic inhibition. *Nat. Commun.* **10**, 1225 (2019).
71. L. A. Slaughter, A. D. Patel, J. L. Slaughter, Pharmacological treatment of neonatal seizures: A systematic review. *J. Child Neurol.* **28**, 351–364 (2013).
72. G. J. Markowitz, S. D. Kadam, D. R. Smith, M. V. Johnston, A. M. Comi, Different effects of high- and low-dose phenobarbital on post-stroke seizure suppression and recovery in immature CD1 mice. *Epilepsy Res.* **94**, 138–148 (2011).
73. J. R. Farwell, Y. J. Lee, D. G. Hirtz, S. I. Sulzbacher, J. H. Ellenberg, K. B. Nelson, Phenobarbital for febrile seizures — Effects on intelligence and on seizure recurrence. *N. Engl. J. Med.* **322**, 364–369 (1990).
74. S. Sulzbacher, J. R. Farwell, N. Temkin, A. S. Lu, D. G. Hirtz, Late cognitive effects of early treatment with phenobarbital. *Clin. Pediatr. (Phila)* **38**, 387–394 (1999).
75. B. J. Sullivan, S. D. Kadam, in *Experimental and Translational Methods to Screen Drugs Effective Against Seizures and Epilepsy* (Humana, New York, NY, 2021), *Neuromethods book series*.

Acknowledgments: We thank S. J. Moss (Tufts University School of Medicine) for the transfer of the S940A^{+/+} and T1007A^{+/+} mice. We thank T. Deeb (Tufts University School of Medicine) and Y. Moore (Tufts University School of Medicine) for useful discussions and technical advice. We thank Y. De Koninck (Université Laval) for sharing aliquots of CLP290. We thank R. Rais' laboratory from the Johns Hopkins Drug Discovery Core for running the HPLC experiments. We thank the journal editors and reviewers. **Funding:** This work was supported by the Eunice Kennedy Shriver National Institute of Child Health and Human Development of National Institutes of Health under grant no. R01HD090884 (S.D.K.). **Author contributions:** S.D.K. conceived the project. B.J.S., P.A.K., B.M.C., L.-R.S., and S.D.K. acquired data. B.J.S., P.A.K., and S.D.K. analyzed data. B.J.S., P.A.K., and S.D.K. wrote the paper. All authors have seen and approved the manuscript. **Competing interests:** S.D.K. is listed as an author on U.S. patent 10525024B2, “Methods for rescuing phenobarbital resistance of seizures by ANA-12 or ANA-12 in combination with CLP290.” All other authors declare that they have no competing interests. **Data and materials availability:** All data needed to evaluate the conclusions in the paper are present in the paper or the Supplementary Materials. S940A^{+/+} and T1007A^{+/+} mice and CLP290 were obtained by material transfer agreements.

Submitted 21 December 2020

Accepted 27 September 2021

Published 9 November 2021

10.1126/scisignal.abg2648